

H-mode transition physics close to double null on MAST and its applications to other tokamaks

H. Meyer 1), P.G. Carolan 1), G.D. Conway 2), G. Cunningham 1), L.D. Horton 2), A. Kirk 1) B. Lloyd 1), R. Maingi 3), F. Ryter 2), S. Saarelma 1), J. Schirmer 2), W. Suttrop 2), H.R. Wilson 1) and the MAST, ASDEX-Upgrade and NSTX teams

1) EURATOM/UKAEA Fusion Association, Culham Science Centre, Abingdon, Oxfordshire, OX14 3DB, UK

2) Max-Planck-Institute for Plasma Physics, Boltzmannstr. 2, 85748 Garching, Germany

3) Oak Ridge National Laboratory, Oak Ridge, Tennessee, 37831, USA

e-mail: Hendrik.Meyer@ukaea.org.uk

Abstract – By accessing extreme parameter regimes combined with well diagnosed edge MAST data contribute towards the understanding of H-mode physics. The first inter-machine comparisons with respect to the influence of the magnetic topology on the power threshold with ASDEX Upgrade and NSTX reveal a reduction of the power threshold in true double null (C-DN) configuration opening new operation regimes in both devices. In L-mode, the negative radial electric field close to the separatrix was found to be more negative in C-DN than in single null (SN), whilst most of the other edge parameters are similar. Pedestal temperatures in MAST are lower than in ASDEX Upgrade in MAST-equivalent discharges, whereas the pedestal densities can be similar, although in long inter ELM periods the MAST density pedestal is higher than on ASDEX Upgrade. In order to test four leading H-mode theories MAST data are compared statistically to their H-mode access criteria. The usual DN operating regime with co current NBI in MAST has been extended to include single null (SN) configurations, to provide more direct comparisons with conventional tokamaks. The plasma edge in SN on MAST is more stable to ELMs and the typical type-III ELMs, often observed in C-DN, are absent, despite input powers close to the H-mode threshold power. In this respect, the stability of measured plasma edge profiles in SN and DN against ideal peeling-ballooning modes will be discussed.

1 Introduction

The H-mode regime [1–3] is the baseline scenario for the next step magnetic confinement fusion device ITER [4]. In H-mode the reduction of turbulent cross field transport inside the edge transport barrier (ETB) leads to the formation of a pedestal in temperature and density with steep gradients in the edge profiles and an improvement in confinement. The steep gradients in H-mode, however, destabilise edge localised modes (ELM) which may reduce the lifetime of the plasma facing components of future larger devices due to the high power efflux during some types of ELMs (type-I). Active or passive control of the pedestal characteristics and hence the ELM may be required in order to mitigate the ELM power or avoid them altogether. An understanding of the physics and conditions leading to the pedestal helps to achieve this goal.

It is widely believed that the reduction of the turbulent transport in H-mode is caused by a sheared $E \times B$ flow in the pedestal region [5, 6]. Such a sheared flow is commonly observed in H-mode [6–8] and can be generated either self-consistently or by imposing a radial electric field at the plasma edge either by biasing [9] or by modification of the toroidal flow [10, 11]. Although, there are many theories dealing with the L/H transition [12, 13], testing them experimentally has proven to be difficult [14–16]. This is mainly because of the many parameters influencing the L/H transition such as plasma geometry and shape [17, 18], the position of the X-point with respect to the ion ∇B -drift direction [1, 17], the refuelling location [11, 19, 20], scrape-off-layer flows [21], and the magnetic topology [22, 23].

For a spherical tokamak such as MAST operation in a double null configuration (DN) with 2 poloidal field nulls (X-points) close to the last closed flux surface (LCFS) is advantageous because of the reduced power flow to the small high field side (HFS) target surfaces. Hence, MAST is mostly operated in DN where an H-mode is commonly achieved [2]. The L/H threshold on MAST is lowest in DN if both X-points are almost on the same flux surface (connected DN, C-DN)[24]. The power needed to achieve H-mode in C-DN is reduced by at least a factor

of 2 compared to single null (SN) or disconnected DN (D-DN) with the ion ∇B -drift towards the X-point on the LCFS [24].

Operation in or close to DN has also been of interest to conventional tokamaks such as ASDEX Upgrade (AUG), JT60-U, DIII-D or JET, since the higher triangularity and elongation used in present day fusion devices has brought the standard SN configuration closer to DN. Furthermore, AUG data suggests that the interesting type-II ELM regime seems to be associated with the closeness of the 2nd X-point to the separatrix [25].

2 Improved L/H threshold in DN

Usually an ETB is formed above a certain threshold, P_{thr} , in power flowing over the LCFS, $P_{\text{loss}} = P_{\text{abs}} + P_{\text{OH}} - dW/dt - P_{\text{rad}}$ (at constant plasma shape), where P_{abs} is the absorbed auxiliary heating power, P_{OH} the Ohmic heating power, dW/dt the rate of change of plasma energy and P_{rad} the radiated power inside the LCFS. In conventional tokamaks the lowest P_{thr} is seen in SN with the ion ∇B -drift towards the X-point. Previously no reduction of P_{thr} in C-DN has been observed in conventional tokamaks [1, 17, 21, 26]. However, the two flux surfaces passing through each X-point need to be almost identical in order to see the effect. On MAST the window of radial separation of the flux surfaces projected to the low field side mid-plane is very narrow $-3 \text{ mm} \leq \delta r_{\text{sep}} \leq 3 \text{ mm}$ [22, 23]. The width is of the order of the ion Larmor radius, ρ_i , or the scrape-off-layer decay length. The accuracy of the equilibrium reconstruction is therefore very important and the window can be easily missed.

Similarity experiments with MAST have been performed on AUG and NSTX. Fig. 1

shows the similarity of the magnetic configurations achieved in these experiments for AUG (left) and NSTX (right). The shape match between AUG and MAST is almost perfect, the former having a slightly lower upper triangularity. Note that the LCFS contour of AUG was shifted by $\Delta R = -0.84 \text{ m}$ and $\Delta Z = -0.09 \text{ m}$ such that the magnetic axes of the two equilibria coincide. The plasma in NSTX is slightly larger than on MAST but with the same shape. This is because with the smaller shape and the feedback gains used the NSTX plasma could not be vertically stabilised to the accuracy needed for these experiments.

On AUG a series of experiments was performed where the plasma was vertically shifted from lower SN (L-SN) via DN to upper SN (U-SN) ($I_p = 0.8 \text{ MA}$, $\bar{n}_e = 4 \cdot 10^{19} \text{ m}^{-3}$, $B_t = -2 \text{ T}$, $\bar{\delta} = 0.28$, $\kappa_{95} = 1.6$, $-15 \text{ mm} \leq \delta r_{\text{sep}} \leq 15 \text{ mm}$). In all discharges the ion ∇B -drift was towards the lower X-point. The plasma was auxiliary heated with ion cyclotron resonance heating (ICRH). The heating power, $P_{\text{ICRH}} = 1.5 \text{ MW}$, was just below the L/H threshold power in lower SN. As can be seen from the increase in line averaged density and stored energy shown in Fig. 2

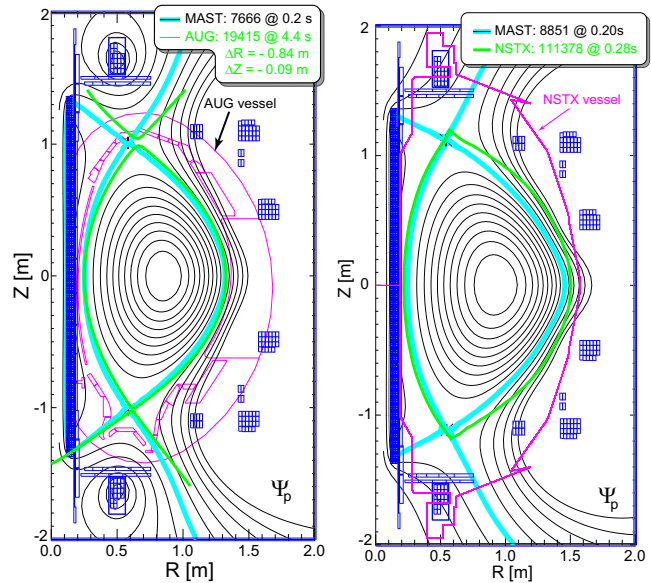


Figure 1: Left: shape comparison between MAST (black, cyan) and AUG (green) similarity discharges. The (R, Z) coordinates of the magnetic axis are mapped on top of each other by shifting the AUG LCFS contour by $\Delta R = -0.84 \text{ m}$ and $\Delta Z = -0.09 \text{ m}$. Right: shape comparison between NSTX (green) and MAST (black, cyan). The vessel contours of AUG and NSTX are indicated in magenta.

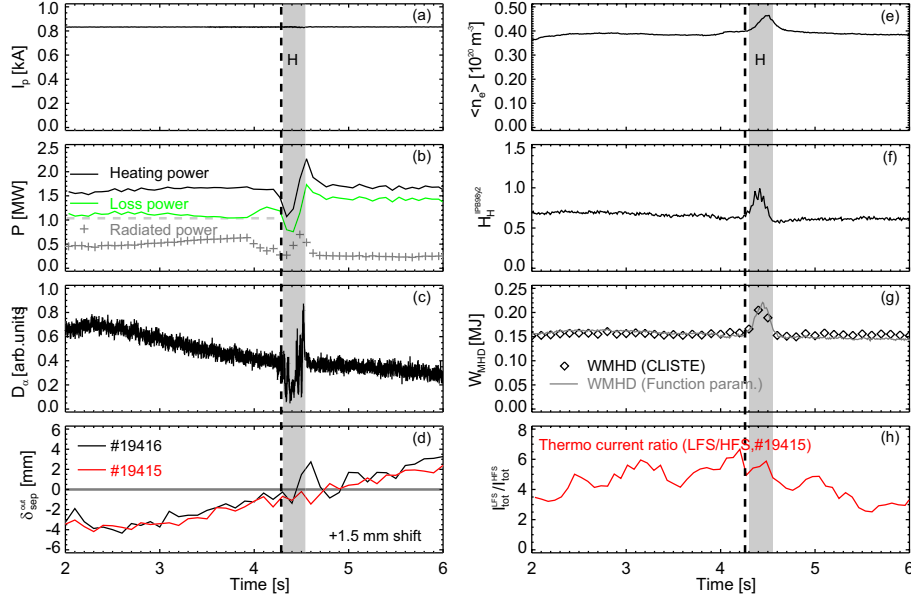


Figure 2: Traces of I_p (a), power (b), D_{α} intensity (c), δr_{sep} (d), \bar{n}_e (e), the IPB H98(y,2) H-factor (f), plasma energy (g) for AUG discharge #19416. The plasma was vertically shifted from LSN to USN to change δr_{sep} . A period of H-mode is highlighted when the plasma is in DN. The ratio of the total thermo current flowing to the LFS targets and the HFS targets (h) and δr_{sep} (c, red) for discharge #19415 which stayed in L-mode because of less auxiliary heating are also shown. The maximum in the thermo current ratio indicates $\delta r_{\text{sep}} = 0$. The traces for δr_{sep} were shifted by 1.5 mm because of the thermo current ratio.

the plasma has ~ 300 ms H-mode period when it passes through DN. By reducing the injected power from $P_{\text{ICRH}} = 1.5$ MW to $P_{\text{ICRH}} = 1.3$ MW H-mode was lost in an otherwise similar discharge. In lower SN ($\delta r_{\text{sep}} = -15$ mm) an H-mode threshold power of $P_{\text{thr}} = (1.17 \pm 0.05)$ MW was measured during consecutive heating ramps using ICRH and neutral beam injection (NBI). In DN, $\delta r_{\text{sep}} = -3$ mm, at 10% higher density, the threshold power is $P_{\text{thr}} = (0.98 \pm 0.05)$ MW.

On NSTX the threshold power in C-DN $P_{\text{thr}} = (0.6 \pm 0.1)$ MW is very similar to MAST [24], showing that the close wall in NSTX has no effect on P_{thr} in C-DN (see Fig. 1). In L-DN, however, H-mode could not be achieved in the similarity experiments despite NBI powers up to $P_{\text{NBI}} = 2$ MW ($P_{\text{loss}} = (1.9 \pm 0.3)$ MW). The reason for that is still unclear since in L-SN a $P_{\text{thr}} = 0.6$ MW has been reported [27]. Furthermore, in the NSTX comparison discharges on MAST H-mode was achieved in L-DN more easily than usual. From the comparisons with NSTX and AUG it is clear that at least a local minimum in P_{thr} exists in C-DN. The minimum is more pronounced in spherical tokamaks than in conventional tokamaks.

As on MAST no significant changes of the T_e and n_e profiles are observed on AUG at the LFS in L-mode as the plasma passes from SN to DN. There is also no indication from the charge exchange measurement on the Lithium beam [28] that the edge ion temperature changes during these scans. However, in both devices a more negative the radial electric field in C-DN compared to L-DN ($\Delta E_r \approx -1$ kV/m) was observed using passive high resolution impurity spectroscopy on MAST and Doppler reflectometry [29] on AUG. The change in E_r on AUG occurs at $\psi_N = 0.96$ and seems to be gradual during the scan reaching its minimum in C-DN. On MAST E_r changes just at or inside the LCFS. The similar magnitude of ΔE_r in MAST and AUG means that $\Delta v_{E \times B} = \Delta E_r / B$ is about a factor of three larger in MAST than in AUG, which could be the reason for the more pronounced reduction of P_{thr} in C-DN on MAST.

Comparing the AUG/MAST similarity discharge (#19416) to a MAST discharge with similar heating power ($P_{\text{NBI}} = 1.8$ MW, $I_p = 0.8$ MA, $\bar{n}_e = 3 \cdot 10^{19} \text{ m}^{-3}$, $B_t = -0.56$ T) similar edge density and temperature profiles can be achieved in L-mode. However, due to the smaller major radius of MAST (AUG: $R = 1.65$ m, MAST: $R = 0.80$ m) similar heating power means that $P_{\text{loss}}/S_{\text{pl}}$ (S_{pl} : plasma surface area) is approximately twice as high on MAST as on AUG to sustain the same T_e profile. In H-mode the temperature and density pedestal on AUG increase by a factor of 2 to $T_e^{\text{ped}} \approx 0.4$ keV and $n_e^{\text{ped}} = 2.5 \cdot 10^{19} \text{ m}^{-3}$ whereas on MAST the change in T_e^{ped} is relatively small ($\Delta T_e \approx 0.05$ keV), although a clear pedestal is established with $T_e^{\text{ped}} = 0.15$ keV, but the density pedestal increases by a factor of 3. Even with comparable H-mode density profiles and similar power levels, pedestal temperatures on MAST are $T_e^{\text{ped}} < 0.2$ keV. Hence, the lower T_e^{ped} on MAST seems to be related to the lower magnetic field. The density pedestal on MAST has a similar width in real space on the LFS and the HFS. The edge density is therefore not constant on flux surfaces supporting an analytical model from DIII-D according to which the density pedestal width is determined by the neutral penetration length [30]. Hence the fuelling location may play an important role and a comparison of the density profiles has to be treated cautiously because of the different fuelling locations on MAST and AUG.

3 Comparison with L/H-threshold theories

In order to compare MAST data statistically with leading H-mode theories all MAST discharges with high resolution TS data [31] of the first three experimental campaigns have been analysed. The LFS edge electron profiles were fitted with a modified tanh fit [32] to calculate edge gradients. Because T_i is not measured in the MAST edge, $T_e = T_i$ was assumed. The data were chosen according to certain quality criteria for the EFIT equilibrium reconstruction and the fit. Using an empirical H-mode indicator based on the edge gradient and D_α emission characteristics, the data were sorted into H-mode, L-mode and transition phases. A similar analysis has been done previously on COMPASS-D [33] and NSTX [16].

The results of this comparison are shown in Fig. 3 for four leading L/H-transition theories: (a) stabilisation of peeling modes [34], (b) suppression of drift-resistive ballooning mode turbulence [35], (c) suppression of drift-Alfén mode turbulence [36] and (d) finite β drift wave turbulence suppression by self generated zonal flows [13]. The comparison is shown at two different radial locations in normalised poloidal flux, $\psi_N = 0.95$ and $\psi_N = 0.98$. For a typical LFS MAST pedestal $\psi_N = 0.95$ is closer to the pedestal top whereas $\psi_N = 0.98$ is close to the point of steepest gradient. For each theory scatter plots of local parameters are shown in a specific parameter space where a clear separation between the L- and H-modes should occur and the parameter region for H-mode is shaded. The points in the transition phase should separate these two regions.

Peeling modes are destabilised by plasma current at the edge and stabilised by the pressure gradient. The current at the plasma edge is dominated by the bootstrap current, j_{BS} , driven by the steep edge pressure gradient. For high collisionality j_{BS} is suppressed. Hence, in a plot of normalised pressure gradient $\alpha_{\text{MHD}} = -Rq^2 \partial \beta / \partial R$ versus edge collisionality $v^* = v_{\text{ei}} L_c / (v_{\text{th}} \epsilon^{3/2})$ ($\beta = p / (2\mu_0 B^2)$, v_{ei} : electron-ion collision frequency, L_c : connection length, v_{th} : thermal velocity of electrons). H-mode points should be located in a region $\alpha_{\text{MHD}} > 0.5$ and $v^* > 1$ according to theory. Fig. 3a shows a clear separation for H- and L-mode values at both flux values. However, the boundary is not marked by the L/H transition points and the theoretically predicted values of α_{MHD} at the transition are too low.

Three dimensional non-linear simulation of electromagnetic drift-ballooning mode turbulence has shown that transport is significantly increased when α_{MHD} exceeds a critical value well be-

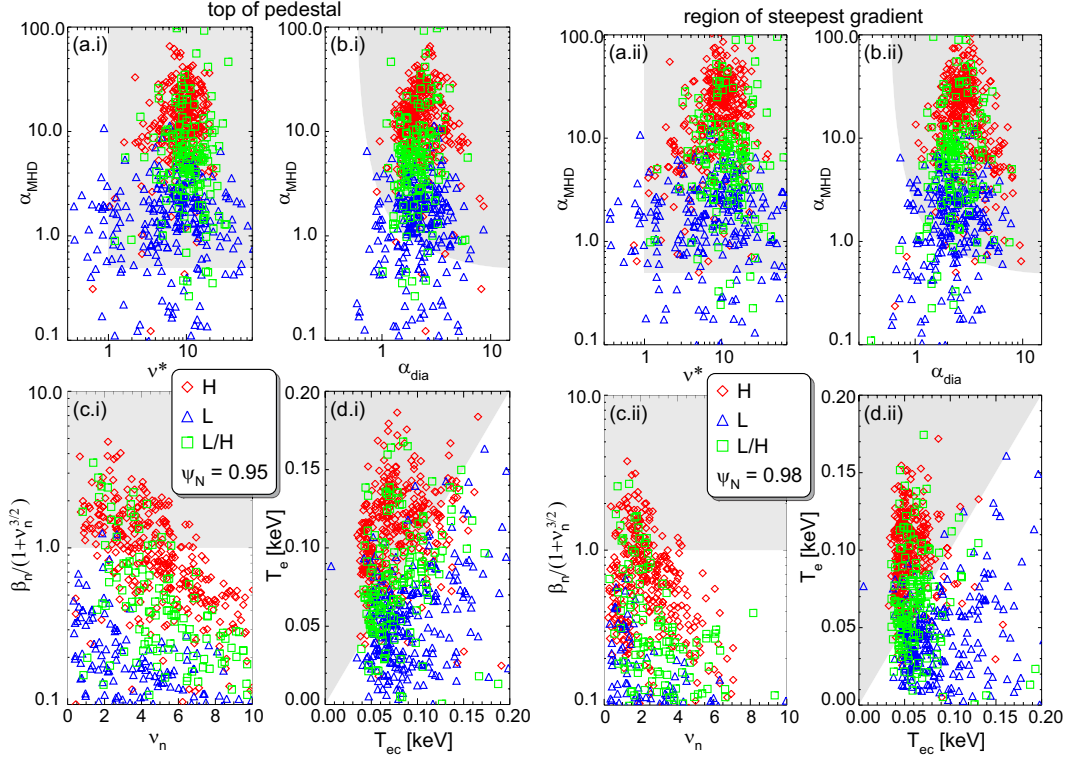


Figure 3: Comparison between experimental data from MAST and theory for (a) peeling modes, (b) drift-resistive ballooning modes, (c) drift Alfvén modes, and (d) zonal flow generation by finite β drift waves at $\psi_N = 0.95$ (left, i) and $\psi_N = 0.98$ (right, ii). The shaded regions indicate where the theories predict H-mode.

low the ballooning limit unless diamagnetic effects are strong. The diamagnetic effects can be characterised by $\alpha_{\text{dia}} = [m_i/(2m_e)]^{(1/4)} [v_{\text{th}}/(v_{\text{ei}}\sqrt{RL_n})]^{(1/2)}/(2\pi q)$ ($L_n = (d \ln n/dR)^{-1}$: density gradient length). The comparison with this theory (see Fig. 3b) is similar to the previous one. L- and H-mode points are well separated and H-mode points are mainly in the predicted region. But again the L/H points don't mark the boundary well.

At the top of the pedestal ($\psi_N = 0.95$, Fig. 3 left) the best separation of all three groups (L, L/H and H) is achieved by the parameter $\beta_n/(1+v_n^{3/2})$ (see Fig. 3c.i) characterising the suppression of long wavelength drift-wave turbulence by the interaction between electron drift waves and Alfvén-waves by coupling through the edge diamagnetic drift velocity. Here, $\beta_n = \sqrt{(m_i/m_e)}\alpha_{\text{MHD}}/(Rdq/dR)$ denotes a normalised pressure gradient and $v_n = v^*[m_i L_p/(m_e R^2 dq/dR)]^{1/2}$ a normalised collision frequency. However, closer to the point of steepest gradient this clear separation is partly lost indicating that other physical processes may become important. The theoretical prediction of $\beta_n > 1 + v_n^{3/2}$ is not confirmed by the MAST data which indicates a boundary of the form $\beta_n > (1 + v_n^{3/2}) \exp\{-m(\psi_N v_n)\}$

At $\psi_N = 0.98$ (Fig. 3 right) the best separation is achieved in Fig. 3d.ii by the critical electron temperature $T_{ec} = \sqrt{L_n} B_t^{2/3} Z_{\text{eff}}^{1/3}/(RM_i)^{1/6}$. For MAST the effective charge $Z_{\text{eff}} = 2$ was assumed and the atomic mass number $M_i = 2$ for deuterium was used for all points. The definition of T_{ec} used here differs from the one given by Guzdar et.al. by a factor of $1/0.45$ [15]. However, with this definition quantitative agreement between theory and experiment is achieved. The difference between experiment and theory might arise from approximations which are only valid

at large aspect ratio and can possibly be resolved in future. The agreement is also reasonable at the top of the pedestal. Note, although the theory distinguishes statistically between L- and H-mode on MAST no change is seen in T_e or T_{ec} on MAST and AUG when the configuration is changed in L-mode from D-DN to C-DN.

4 Pedestal stability against peeling-ballooning modes

Although, peeling-ballooning modes seem to be of minor relevance to the L/H transition, they are the most promising candidate for ELM triggers. On MAST so far no ELMs have been observed in D-DN or SN configurations, whereas in C-DN ELMs are commonly observed under similar conditions [37]. Therefore, the influence of the proximity of a 2nd X-point on the ideal MHD stability at the edge was investigated using MAST equilibria and experimental electron profiles. The stability of peeling-ballooning modes was studied for medium toroidal mode numbers ($6 \leq n \leq 14$) using the ELITE code [38]. The equilibrium was calculated with the fixed boundary code HELENA [39] using kinetic profiles from TS measurements and plasma boundary from EFIT reconstruction. Experimental data suggest that the toroidal mode number for ELMs on MAST is around 12 [40]. Peeling modes are edge kink instabilities resonant to rational surfaces just outside the plasma edge and are thought to play a key role in ELMs. They are stabilised by a pressure gradient and destabilised by the parallel current density. Ballooning modes on the other hand are driven unstable by an increasing pressure gradient, whereas an increase in parallel current density is stabilising by enabling access to second stability.

The stability calculations were done for two real and one artificial MAST discharges: The C-DN discharge #8209 ($I_p = 0.75$ MA, $B_t(R = 0.76 \text{ m}) = 0.56$ T, $\bar{n}_e = 5.4 \times 10^{19} \text{ m}^{-3}$, $P_{\text{NBI}} = 2.4$ MW), the L-SN discharge #7508 ($I_p = 0.52$ MA, $B_t(R = 0.76 \text{ m}) = 0.53$ T, $\bar{n}_e = 3.6 \times 10^{19} \text{ m}^{-3}$, $P_{\text{NBI}} = 1.2$ MW), and an artificially derived L-SN equilibrium by modifying the C-DN equilibrium from discharge #8209 using the same edge profiles as in the C-DN case. The kinetic profiles were taken from the high resolution TS system assuming $T_i = T_e$. In discharge #8209 the TS measurement was taken 0.5 ms before an ELM after a 5 ms inter ELM period. In discharge #7508 the TS measurement was taken 20 ms into a 25 ms ELM free H-mode. Since the gradient at the LFS is underestimated for steep gradients because of the diagnostic resolution, measurements from the HFS are used. In addition, an artificial L-SN discharge was created by changing the C-DN equilibrium to L-SN whilst retaining the kinetic profiles from the real C-DN discharge. This allows to study the effect of the magnetic configuration on the stability alone. The parallel current at the edge is dominated by the bootstrap current, j_{BS} , in H-mode. Here, the expression from Sauter et.al. is used [41].

Note, that ELITE cannot handle the separatrix but can approach diverted plasmas very closely. The magnetic field around the X-point is stochastic and the safety factor at the q_{edge} at the edge is finite but not well defined. Therefore, a narrow region at the edge has to be removed from the equilibrium reconstruction allowing a more or less arbitrary variation of q_{edge} . This has implications on the peeling mode stability which is sensitive to $0 < \Delta = m - nq_{\text{edge}} < 1$ (m, n : poloidal and toroidal mode number respectively). For $\Delta \leq 0.1$ the plasma can be unstable to very narrow peeling-modes, but stable against all modes with higher Δ . The arbitrariness of q_{edge} means two things; On the one hand that such modes can always be found in the analysis and on the other hand that slight changes in the equilibrium will stabilise such modes. Only modes with a wide mode structure which are unstable for a number of values of Δ are likely to trigger ELMs. Hence, all other modes are neglected as ELM triggers. Similar investigations for lower mode numbers for ASDEX-Upgrade using the GATO code found DN to be more stable than SN [42]. There, the radial extent of the modes was found to be much smaller in DN than in SN, consistent with the occurrence of type-II ELMs in these regimes.

From the experimental data the position of the edge transport barrier (ETB), ψ_N^{ETB} , (position of steepest pressure gradient) with respect to the LCFS is only known to a certain accuracy. However, the edge stability is very sensitive to this relative position as can be seen from Fig. 4. Here, the the growth rates of the $n = 6$ mode are shown function of ψ_N^{ETB} for different Δ for MAST discharge #8209. Experimentally the ETB is located at $\psi_N^{\text{ETB}} = 0.987$ and only an increase of the pressure pedestal from $p_e^{\text{ped}} = 1.95$ kPa to $p_e^{\text{ped}} = 3.1$ kPa destabilises the edge. For $\psi_N^{\text{ETB}} = 0.995$, however, the $n = 6$ mode is unstable for a wide range of Δ . The mode structure spans the whole pedestal region and is poloidally localised around the X-points. The stability for the experimental C-DN and the artificial L-SN equilibrium is very similar. Hence, on MAST the 2nd X-point has no influence on the peeling-ballooning stability at medium n numbers. The edge of the experimental SN discharge (#7508) was found to be ideal MHD stable for p_e^{ped} up to 3 kPa (the experimental value of $p_e^{\text{ped}} = 1.5$ kPa) and is not destabilised by moving ψ_N^{ETB} closer to the LCFS.

The absence of ELMs in SN on MAST under conditions where ELMs are observed in C-DN together with the similar stability of C-DN and L-SN equilibria with the same edge profiles suggest that there is a mechanism in SN, which prevents the profiles to reach their stability limit. Multi-time TS shows, that in long ELM-free periods in L-SN the pressure pedestal saturates.

5 Conclusions

The comparison of similar discharges in MAST and AUG as well as MAST and NSTX showed that there is at least a local minimum of the L/H threshold in connected double null (C-DN) compared to lower single null (L-SN). The reduction of P_{thr} in MAST and NSTX is more pronounced than in ASDEX Upgrade (AUG). The change of the configuration from L-SN to C-DN gives rise to a more negative radial electric field, E_r , in L-mode inside the last closed flux surface. The change of E_r in MAST and AUG was of similar magnitude, hence, the change in the $E \times B$ velocity in MAST is larger than in AUG, which may be the reason for the more pronounced reduction of P_{thr} between L-SN and C-DN in spherical tokamaks. The similar P_{thr} in C-DN in MAST and NSTX shows that the wall has no significant effect on P_{thr} .

On MAST similar edge density and temperature profiles as in AUG can be achieved in L-mode with similar heating powers. In H-mode, however, the pedestal temperature on AUG is about 2.7 times higher than on MAST, but the pressure pedestals are similar. Nevertheless, even in similar MAST discharges with similar density pedestals as on AUG, T_e^{ped} is less than 0.2 keV supporting a scaling of T_e^{ped} with the magnetic field.

On the one hand, MAST data support statistically the theory by Guzdar et.al. for the L- to H-mode transition based on finite β drift wave stabilisation by self generated flow shear. Agreement with the theory is achieved, but only with a critical electron temperature, T_{ec} , twice as high as theoretically predicted. On the other hand, neither T_{ec} nor T_e change in L-mode between C-DN and L-SN, although this configuration change leads to an L/H transition at slightly higher power. Hence, an element of the the physics leading to the easier H-mode access in C-DN is

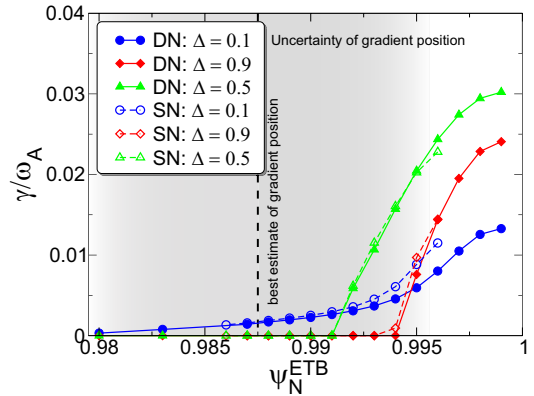


Figure 4: Normalised growth rate of $n = 6$ peeling-ballooning mode as a function of pedestal pressure position for MAST discharge #8209 with a C-DN (solid) and an artificial L-SN (dashed) equilibrium.

either missing or the statistical agreement shows only the features of H-mode rather than the cause.

MAST H-mode edge profiles close to an ELM crash in a C-DN discharge were found to be unstable to ideal MHD peeling-ballooning modes at medium toroidal mode numbers. Removing the second X-point from the LCFS in the model has no effect on the stability and mode structure. The profiles in the ELM free H-mode of an L-SN discharge, however, were found to be far from the stability boundary. Hence, the absence of ELMs in L-SN observed so far is caused by the mechanisms determining the edge pedestal, which seem to be different in L-SN and C-DN.

Acknowledgements: This work was jointly funded by the UK Engineering and Physical Sciences Research Council and EURATOM.

References:

- [1] ASDEX-TEAM, Nucl. Fusion **29** (1989) 1959.
- [2] AKERS, R. J. et al., Phys. Rev. Lett. **88** (2002) 035002.
- [3] MAINI, R. et al., Phys. Rev. Lett. **88** (2002) 35003.
- [4] ITER-TEAM, *ITER Physics Basis*, volume 39, chapter 2, pages 2175–2249, Nucl. Fusion, 1999.
- [5] HAHM, T. S. et al., Physics of Plasmas **2** (1995) 1648.
- [6] BURRELL, K. H., Phys. of Plasmas **6** (1999) 4418, Invited contribution to the APS-meeting 1999 in Atlanta.
- [7] MEYER, H. et al., Czechoslovak Journal of Physics **50** (2000) 1451.
- [8] CAROLAN, P. G. et al., Rev. Sci. Instr. **72** (2001) 881.
- [9] WEYNANTS, R. R. et al., Plasma Phys. Control. Fusion **40** (1998) 635.
- [10] FÜLÖP, T. et al., Phys. Rev. Lett. **89** (2002) 225003.
- [11] FIELD, A. R. et al., Plasma Phys. Control. Fusion **46** (2004) 981.
- [12] CONNOR, J. W. et al., Plasma Phys. Control. Fusion **42** (2000) R1.
- [13] GUZDAR, P. N. et al., Phys. Rev. Lett. **87** (2001) 15001.
- [14] CARLSTROM, T. N. et al., Nucl. Fusion **39** (1999) 1941.
- [15] GUZDAR, P. et al., Phys. Rev. Lett. **89** (2002) 265004.
- [16] KAYE, S. M. et al., Phys. of Plasmas **10** (2003) 3953.
- [17] CARLSTROM, T. N. et al., Plasma Phys. Control. Fusion **36** (1994) A147.
- [18] ANDREW, Y. et al., Plasma Phys. Control. Fusion **46** (2004) A87.
- [19] GOHIL, P. et al., Phys. Rev. Lett. **86** (2001) 644.
- [20] VALOVIČ, M. et al., in *28th European Physical Society Conference on Controlled Fusion and Plasma Physics*, 2001.
- [21] LABOMBARD, B. et al., 16th Int. Conf. on Plasma Surface Interactions in Controlled Fusion Devices (Portland, USA 24–28 May 2004) P2-57, to be published in J. Nucl. Mat.
- [22] MEYER, H. et al., in *29th European Physical Society Conference on Controlled Fusion and Plasma Physics*, volume 26B, European Physical Society, 2002.
- [23] AKERS, R. J. et al., Physics of Plasmas **9** (2002) 3919.
- [24] MEYER, H. et al., Plasma Phys. Control. Fusion **46** (2004) A291.
- [25] STOBER, J. et al., Nucl. Fusion **41** (2001) 1123.
- [26] CARLSTROM, T. N. et al., Plasma Phys. Control. Fusion **40** (1998) 669.
- [27] BUSH, C. E. et al., Phys. of Plasmas **10** (2003) 1755.
- [28] REICH, M. et al., Plasma Phys. Control. Fusion **46** (2004) 797.
- [29] CONWAY, G. et al., Plasma Phys. Control. Fusion **46** (2004) 951.
- [30] GROEBNER, R. et al., Technical Report GA-A24130, General Atomics, 2002.
- [31] WALSH, M. J. et al., Rev. Sci. Instr. **74** (2003) 1663.
- [32] GROEBNER, R. J. et al., Plasma Phys. Control. Fusion **40** (1998) 673.
- [33] FIELD, A. R. et al., J. Plasma Fusion Res. **4** (2001) 234.
- [34] WILSON, H. et al., Phys. of Plasmas **6** (1999) 1925.
- [35] ROGERS, B. et al., Phys. Rev. Lett. **81** (1998) 4396.
- [36] KERNER, W. et al., Contrib. Plasma Phys. **38** (1998) 118.
- [37] KIRK, A. et al., Nucl. Fusion **46** (2003) 551.
- [38] WILSON, H. R. et al., Phys. of Plasmas **9** (2002) 1277.
- [39] HUYSMANS, G. et al., in *CP90 Conf. on Comput. Phys.*, edited by TENNER, A., pages 371–376, World Scientific, Singapore, 1991.
- [40] KIRK, A. et al., Phys. Rev. Lett. **92** (2004) 245002.
- [41] SAUTER, O. et al., Phys. of Plasmas **9** (2002) 5140.
- [42] SAARELMA, S. et al., Nucl. Fusion **43** (2003) 261.